Mesh dependence analysis for simulating unsteady cavitation around a plane convex hydrofoil

Mesh dependence analysis for simulating unsteady cavitation around a plane convex hydrofoil

D Puga[1], X Escaler[2], V Hidalgo[3] and X Luo[1]

[1]State Key Laboratory of Hydro Science & Engineering, Department of Energy and Power Engineering, Tsinghua University, Beijing 100084, China
[2] Barcelona Fluids & Energy Lab., Universitat Politécnica de Catalunya, Barcelona 08028, Spain
[3] Laboratorio de Informática-Mecánica, Escuela Politécnica Nacional, Quito 170525, Ecuador

E-mail: dnd20@mails.tsinghua.edu.cn

Abstract. The mesh significantly influences the quality of the numerical results in computational fluid dynamics (CFD) problems due to its correlation with turbulence models. In the present paper a structured mesh was generated using Gmsh and two semi-structured meshes were generated using snappyHexMesh to determine the suitable mesh distribution for simulating unsteady cavitation around a plane convex hydrofoil. The numerical simulation was conducted by using the software OpenFOAM with the *k-ω* SST SAS turbulence model and the Zwart-Gerber-Belamri (ZGB) cavitation model. Besides, the experimental results obtained by the Laboratory for Hydraulic Machines of École Polytechnique Fédérale de Lausanne were used to validate the numerical results. The results showed that both structured and semi-structured meshes predicted the cavitation pattern and the maximum cavity length. The semi-structured mesh with suitable refinement reproduced in detail the dynamic behavior of unsteady cavitation, while the structured mesh efficiently reproduced the phenomenon.

1. Introduction

In CFD modelling, mesh generation leads to either success or failure of the numerical simulation due to the mesh quality significantly impacts on the accuracy of the solution and influences the computational cost required to solve the study case [1,2]. An adequate mesh should satisfy some quality metrics such as non-orthogonality, cell skewness, aspect ratios, smoothing among others to guarantee its properly operation and optimize computational resources during the simulation [2–4]. Also, throughout y^+ criteria wall modelling validity is assessed only after the simulation has been run [2]. Thus, different mesh types have been emerged to discretize the domain showing inherent advantages and disadvantages. For example, structured meshes main characteristics are robustness and accuracy but the generation process is complex and requires expertise [5]. Whereas, semi-structured meshes show easy mesh generation for complex geometries and adaptability to local features of interest [6].

CFD has been widely used to obtain detailed information related to cavitation behavior applying different turbulence models to enhance the numerical results. The required mesh quality varies according to the turbulence modelling requirements. In fact, Large Eddy Simulation (LES) turbulence models tie very closely with mesh aspects and require higher mesh quality levels than that for Reynolds Averaged

Navier-Stokes (RANS) methods [2]. Therefore, a hybrid RANS-LES turbulence model Scale Adaptive Simulation (SAS) was proposed, where the stable flow regions are covered by RANS and the turbulent spectrum is treated by LES. The advantage of the SAS turbulence model is that does not show an explicit influence of the grid spacing on the RANS mode of the model [7].

In the present paper, a structured mesh and two semi-structured meshes are adopted to analyze their applicability to conduct numerical simulations by using *k-ω* SST SAS turbulence model to study unsteady cavitation around a plane convex hydrofoil.

2. Model description

2.1. Scale Adaptive Simulation (SAS)

The viscous stress tensor τ'_{ij} in the *k-ω* SST SAS turbulence model [8] is calculated as equation (1).

$$\tau'_{ij} = \mu_T \left(2\bar{S}_{ij} - \frac{2}{3}\delta_{ij}\bar{S}_{kk} \right) \tag{1}$$

where μ_T is the turbulent viscosity coefficient, $\bar{S}_{ij}$ is the strain rate tensor and δ_{ij} is the Kronecker's delta. The von Karman length scale L_{vK} is used to modify the length scale in SAS as equation (2) [7,8]. κ is the von Karman constant 0.41 [8], and *k* is another subscript for space in the partial derivatives of velocity components [9].

$$\begin{gathered} L_{\mathrm{vK}} = \kappa \left| \frac{\partial U/\partial y}{\partial^2 U/\partial y^2} \right|, \\ \frac{\partial U}{\partial y} = S = \sqrt{2 S_{ij} S_{ij}}\ ;\ S_{ij} = \frac{1}{2}\left(\frac{\partial U_i}{\partial x_j} + \frac{\partial U_j}{\partial x_i} \right), \\ \frac{\partial^2 U}{\partial y^2} = \sqrt{\frac{\partial^2 U_i}{\partial x_k^2}\frac{\partial^2 U_i}{\partial x_j^2}} \end{gathered} \tag{2}$$

2.2. Zwart-Gerber-Belamri cavitation model (ZGB)

In the present study ZGB cavitation model was updated and implemented for OpenFOAM version 6 based on the previous study [9]. The ZGB model is shown in equation (3).

$$\dot{m} = \begin{cases} \dot{m}^+ = F_{\mathrm{v}} \dfrac{3 r_{\mathrm{nuc}}(1-\alpha)\rho_{\mathrm{v}}}{R_{\mathrm{B}}} \sqrt{\dfrac{2}{3}\dfrac{p_{\mathrm{v}} - p}{\rho_{\mathrm{l}}}} & if\ p \le p_{\mathrm{v}} \\ \dot{m}^- = -F_{\mathrm{c}} \dfrac{3\alpha\rho_{\mathrm{v}}}{R_{\mathrm{B}}} \sqrt{\dfrac{2}{3}\dfrac{p - p_{\mathrm{v}}}{\rho_{\mathrm{l}}}} & if\ p > p_{\mathrm{v}} \end{cases}, \tag{3}$$

where $\dot{m}$ is the interphase mass transfer rate per unit volume equal to $\dot{m}^+ - \dot{m}^-$, $\dot{m}^+$ is the evaporation mass source and $\dot{m}^-$ is the condensation mass source during phase changes [10]. *p* is the pressure, *α* is the vapor volume fraction, and *ρ* is the density. The subscripts l and v are for liquid and vapor in the vapor-water mixture. The calibration constant for vaporization (F_{v}) and that for condensation (F_{c}) are set in the values that gave the best results according to the reference [11]. Therefore, F_{v} is 300 and F_{c} is 0.03. The nucleation site fraction (r_{nuc}) is 5×10^{-6} and R_{B} is the typical bubble radius size in water.

2.3. OpenFOAM setup

OpenFOAM version 6, GNU/Linux ArchLinux with kernel Linux 5.13.10-arch1-1 (x86 64) and XFCE desktop were used. The pressure-velocity coupling algorithm was PIMPLE, the time discretization scheme was Euler scheme, and the spatial discretization scheme was Gauss linear upwind scheme. The simulation was run in parallel through simple decomposition method and the openMPI implementation. Thus, the computational domain was decomposed in sixteen subdomains to run in an INTEL processor with 1.3 GB/124 GB RAM memory and execution time 24 304.3 s for the structured mesh (hereafter case A) and 7 GB/124 GB RAM memory and execution time 107 428 s for the semi-structured meshes (hereafter case B and case C) at Laboratorio de Informática-Mecánica of Escuela Politécnica Nacional.

3. Geometric model and mesh generation

3.1. Geometric model

Based on a previous study [12], figure 1a shows the plane convex hydrofoil used in the present research. The chord length c is 91.1 mm and the attack angle $(\widehat{AOB})$ is 3°. Figure 1b shows the computational domain, where the front and the back planes are set as symmetry, and the top, the bottom and the hydrofoil surface are set as no-slip walls. The domain inlet velocity is U_{inlet} = 35 m s^{-1} and the domain outlet pressure is P_{outlet} = 613.575 kPa.

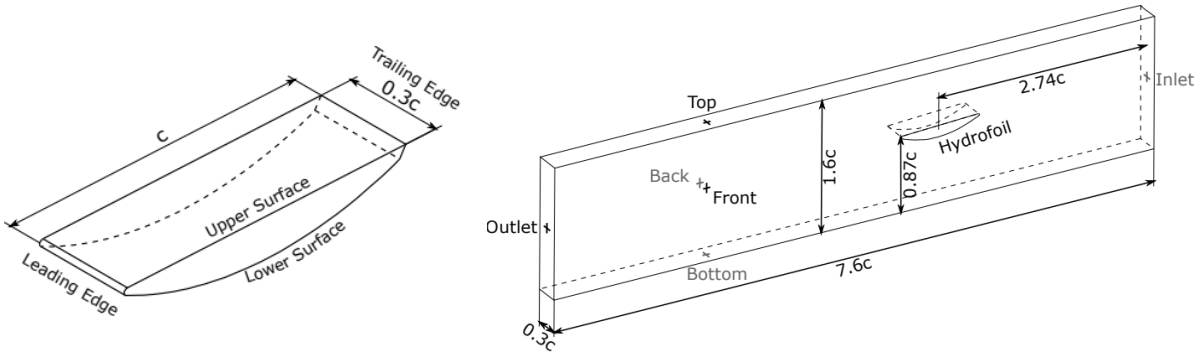

(a) (b)

Figure 1. (a) Plane convex hydrofoil [12], (b) Computational domain.

3.2. Mesh generation

Figure 2a shows the methodology for a structured mesh (case A) generation using Gmsh 4.6.0. The first step was to obtain the Cartesian coordinates of the hydrofoil and the computational domain to define the geometry. Second, plane surfaces, nodes number and geometric progressions were defined. Then, the planar geometry was extruded to get a three-dimensional domain. Also, the boundary conditions were set. Finally, the structured mesh was generated.

Figure 2b shows the methodology for semi-structured meshes (cases B and C) generation using snappyHexMesh. A background mesh was generated using blockMesh. The hydrofoil geometry was included as a .stl file. Then, using snappyHexMesh a refinement box was generated in the vicinity of the hydrofoil where the background mesh was split in small cells and the hydrofoil surface was refined at a finer refinement level than that of the refinement box. The cells inside the hydrofoil surface were removed and fitted around the hydrofoil border. Finally, three layers were introduced along the border surface of the hydrofoil to improve the wall model.

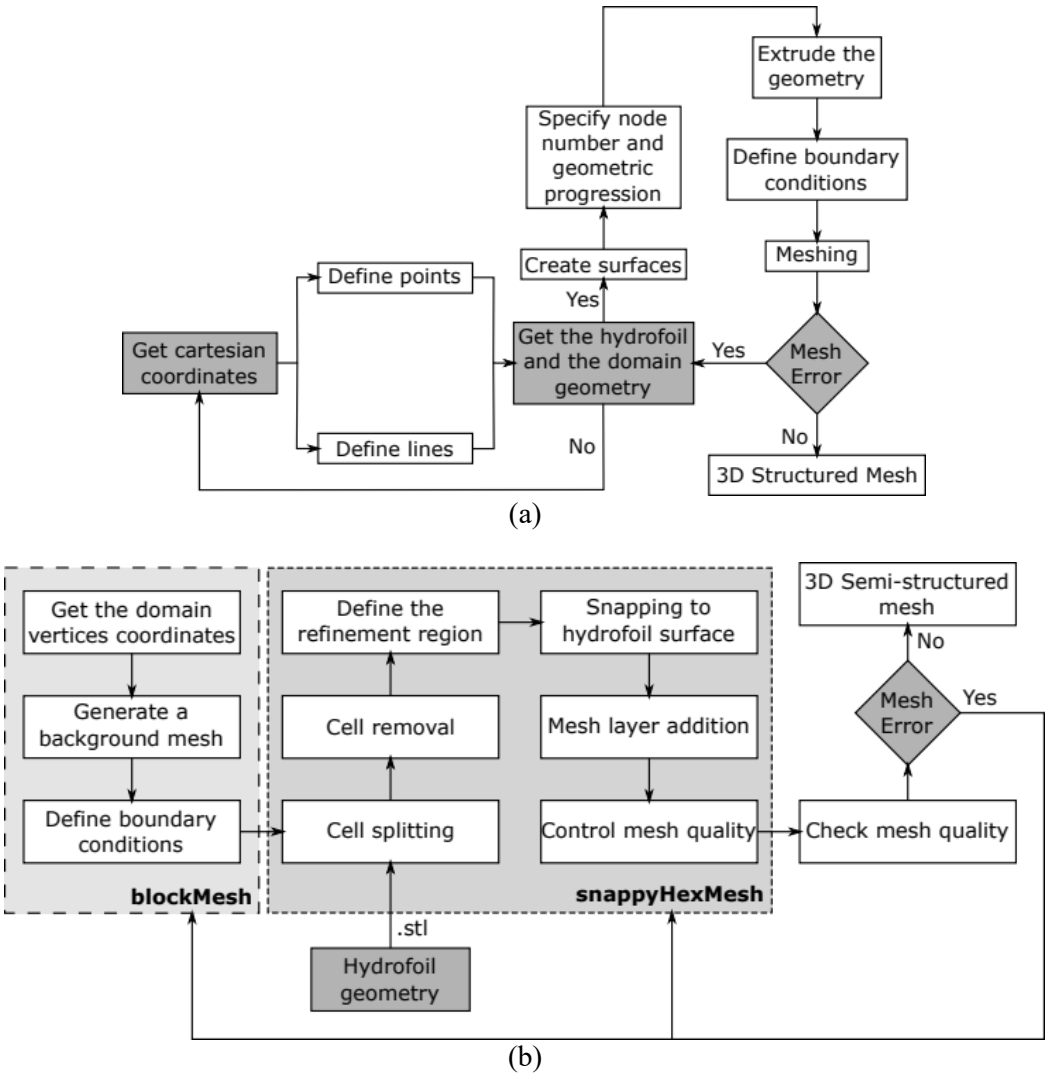

Figure 2. (a) Structured mesh generation methodology, (b) Semi-structured mesh generation methodology.

Figure 3a shows the structured mesh (case A) where the domain was decomposed in eleven blocks with separate meshes. Blocks 2 and 3 show a "C" type mesh around the leading edge, and the other blocks show an "H" type mesh. Besides, an exponential distribution refinement was applied, where the smaller cells are located near the hydrofoil surface and the bigger cells are located far from the hydrofoil surface. The span-wise direction has 40 layers according to a previous study [9]. On the other hand, the semi-structured meshes have a refinement box and local refinement with three layers around the hydrofoil surface. Furthermore, the background mesh of the case B has one block with hexahedral elements and the cell expansion ratio is 1 in all directions as figure 3b shows. Also, figure 3c shows the background mesh of the case C that has three blocks with hexahedral elements. The cell expansion ratio of the first block is 4 in x direction, that for the second block is 1 in all directions and that for the third block is 0.4 in x direction. In cases B and C, the span-wise direction has 40 layers only inside the refinement box according to [9]. As a result, the case A mesh is a multiblock mesh with exponential refinement, the case B mesh has one block with a refinement box, local refinement and layers, and the case C mesh is a multiblock mesh with a refinement box, local refinement, layers and exponential refinement in x direction.

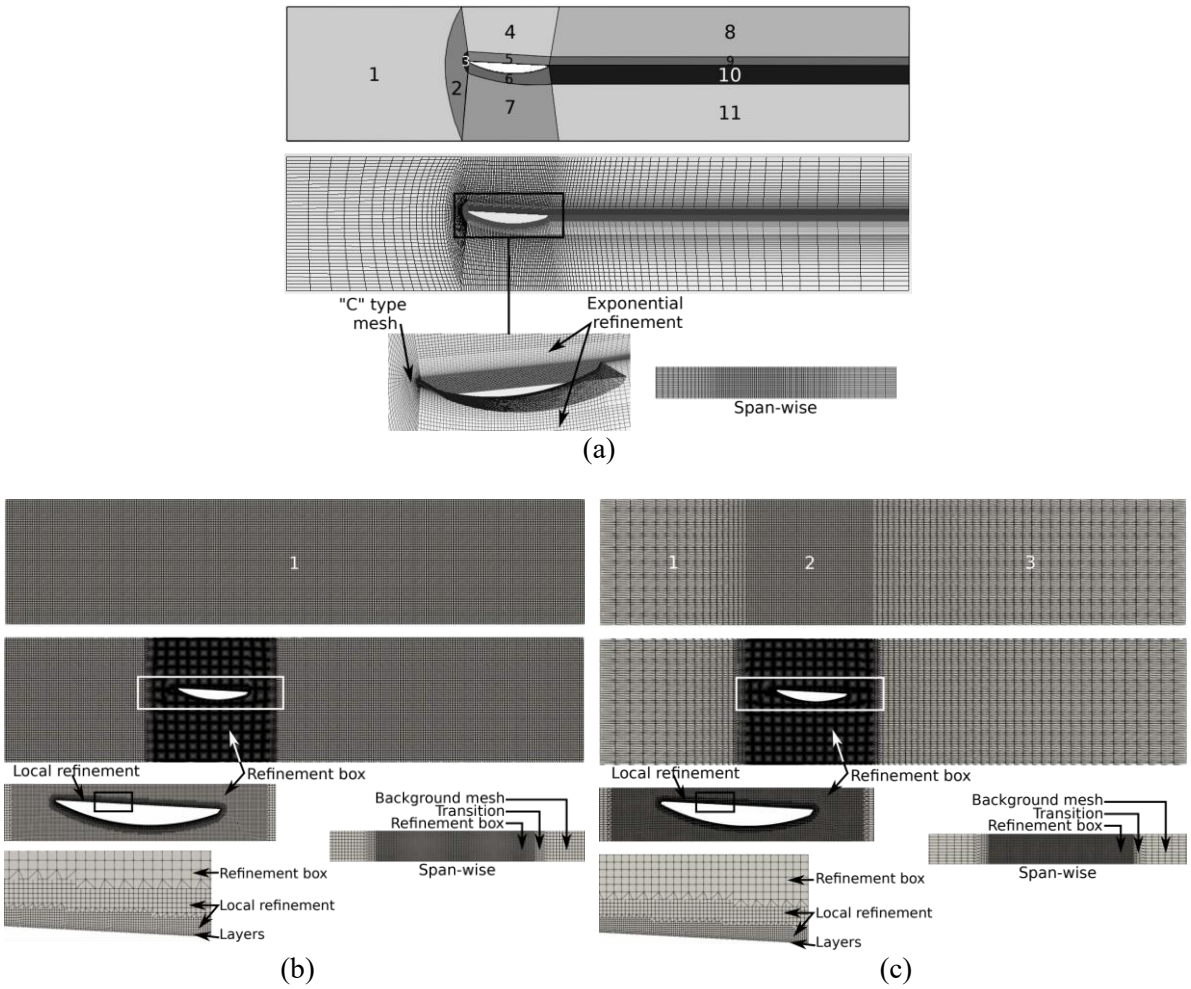

Figure 3. Mesh (a) Case A, (b) Case B, (c) Case C.

4. Results and discussion

Table 1 shows the number of elements per element type and the node number for cases A, B and C.

Table 1. Mesh elements.

Object	Case A	Case B	Case C
Nodes	558 420	4 032 318	4 072 027
Quadrangles	48 066	-	-
Hexahedra	534 120	3 675 363	3 720 890
Prisms	-	25 280	25 280
Polyhedral	-	71 260	71 420
Total	582 186	3 771 903	3 817 590

The main difference between the structured and the semi-structured meshes is their composition. The structured mesh has only quadrangles and hexahedra, and the semi-structured meshes have hexahedra, prisms and polyhedral elements.

Dimensionless parameters such as the omega number and y^+ assess the mesh quality. The omega number (Ω) shows the relation between the elements number (NE) and the nodes number (NN) as equation (4) [13,14].

$$\Omega = \frac{NE}{NN} \tag{4}$$

The y^+ around the hydrofoil surface was calculated as equation (5) shows.

$$y^+ = \frac{u_\tau y}{v}, \tag{5}$$

where u_τ is the friction velocity, y is the distance to the nearest hydrofoil wall and v is the fluid kinematic viscosity.

Table 2 shows the dimensionless parameter values for cases A, B and C. Ω is similar in all cases, this means that the three meshes have almost the same number of elements per node and consumes almost the same amount of computational resources to achieve the numerical result. Moreover, $y^+ < 5$ lies in the viscous sublayer, $5 \leq y^+ < 30$ lies in the buffer layer, and $30 \leq y^+ < 300$ lies in the fully turbulent region [15,16]. In all cases, y^+ min values lie in the viscous sublayer region. y^+ max values in all cases and y^+ average values for cases B and C lie in the fully turbulent region. Finally, y^+ average for case A lies in the buffer layer region.

Table 2. Dimensionless parameters.

Parameter	Case A	Case B	Case C
Ω	1.043	0.935	0.938
y^+ max	38.100	104.105	102.112
y^+ min	2.620	1.490	1.323
y^+ average	22.060	45.191	47.177

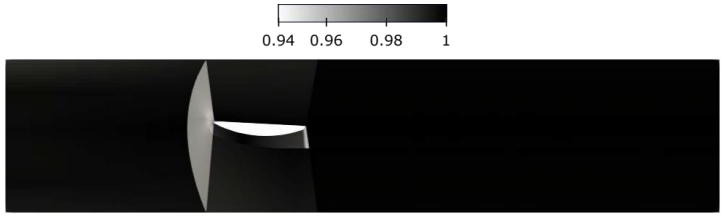

(a)

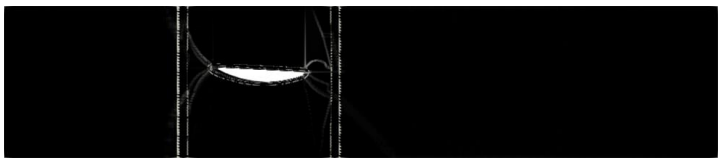

(b)

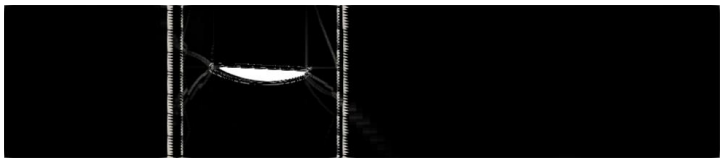

(c)

Figure 4. Hexahedral distortion (a) Case A, (b) Case B, (c) Case C.

Moreover, the hexahedral distortion was analyzed using the quality mesh filter of Paraview due to most elements of structured and semi-structured meshes are hexahedral. The hexahedral distortion acceptable range is between 0.5 and 1 [17].

Figure 4 shows that the hexahedral distortion for all cases is within the acceptable range with values between 0.94 and 1. Figure 4a shows the case A hexahedral distortion analysis where the lowest value is located in the "C" type mesh around the leading edge and in the trailing edge of the hydrofoil. The hexahedral distortion analysis of cases B and C are shown in figures 4b and 4c where the lowest value is located in the refinement box edges, the leading and trailing edges, and in the local refinement of the hydrofoil surface. In fact, case C shows more hexahedral distortion than case B.

Further analysis of the cavitation pattern and the maximum cavity length is shown in figure 5 to validate the numerical results. The cavitation pattern of cases A, B and C is shear cavitation according to the attack angle ($\widehat{AOB} = 3°$) and the cavitation number ($\sigma = 1$) [18]. Shear cavitation is related to the turbulent structure of shear flows where rotational structures develop. In case A the cavity seems like a film and that for cases B and C show a more realistic structure. In all cases, the re-entrant jet cannot achieve the leading edge because the shedding occurs after the cavity reached its maximum length. In cases B and C the beginning of shedding process is clearer than in case A. The predicted cavity pattern has good agreement with the experimental result in all cases. However, the simulations do not predict the small cavity detachments that the experimental result shows. The predicted maximum cavity length in case A is 26.65 mm, in case B is 26.29 mm, and in case C is 25.99 mm. The experimental maximum cavity length is 27.62 mm.

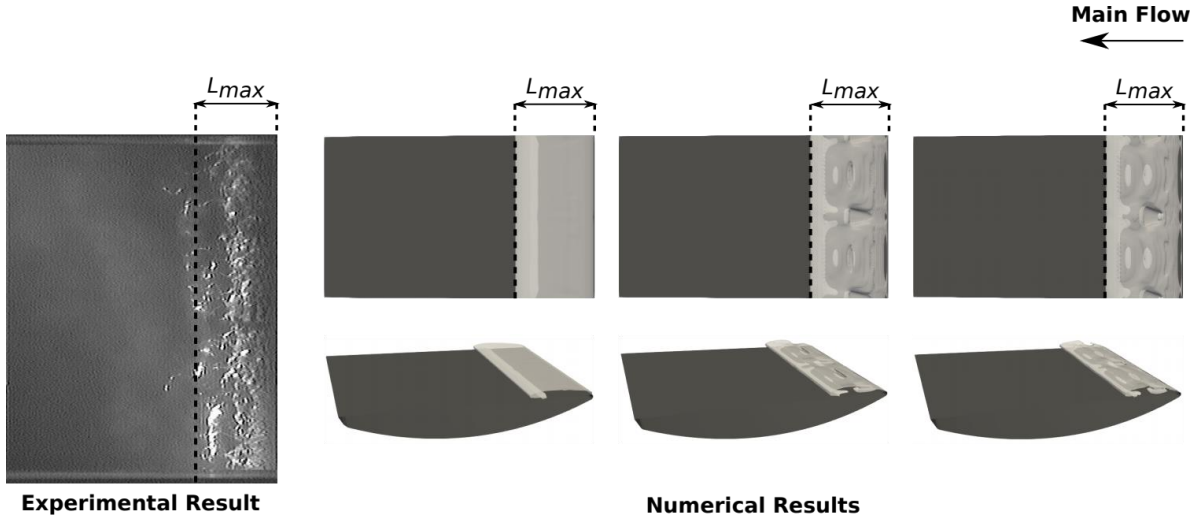

Figure 5. (a) Experimental result [19], and cavity iso-contours at α = 0.1 (b) Case A at t = 0.0022 s, (c) Case B at t = 0.0026 s, (d) Case C at t = 0.0026 s.

Table 3 shows the estimated error as equation (6) to measure the difference between the experimental and the numerical results.

$$Error = \left| \frac{\left(L_{max}/c\right)_{\text{Exp.}} - \left(L_{max}/c\right)_{\text{Num.}}}{\left(L_{max}/c\right)_{\text{Exp.}}} \right| \times 100 \quad (6)$$

Table 3. Numerical and experimental results based on L_{max}.

Case	L_{max}/c		Error (%)	f (Hz)	St
	Num.	Exp.			
A	0.293		3.53	234.90	0.18
B	0.289	0.303	4.83	201.34	0.15
C	0.285		5.93	227.27	0.17

The estimated error shows agreement between the experimental and the numerical results in all cases when the maximum cavity length is analyzed. The cavity oscillation frequency and the Strouhal number show minimum variation between the three cases.

5. Conclusion

The meshes of cases A, B and C satisfactorily reproduced the unsteady cavitation around the plane convex hydrofoil using the *k-ω* SST SAS turbulence model when the cavitation pattern and the maximum cavity length were compared. However, based on the analysis of the dimensionless parameters the structured mesh shows better qualities than the semi-structured meshes. In fact, the semi-structured meshes have almost eight times more elements than the structured mesh which means that the time required to achieve the numerical result is greater for the semi-structured meshes compared with that for the structured mesh. Besides, y^+ min and y^+ average values of the structured mesh allow cavitation studies into the viscous sublayer and into the buffer layer regions. Moreover, the hexahedral distortion in the semi-structured meshes is in the transition zones between the refinement levels which is not desirable. Finally, the error between the experimental and the numerical results, the cavity oscillation frequency and the Strouhal number in all cases are almost the same, and the semi-structured meshes show a more realistic shear cavitation pattern. In this context, the use of the structured mesh is highly recommended to obtain high quality results at a low computational cost to solve engineering problems where the time is a limited resource by using the *k-ω* SST SAS turbulence model, and the use of the semi-structured meshes is recommended when a detailed study of the dynamic behavior of unsteady cavitation is required.

Acknowledgements

The present research was financially supported by the National Natural Science Foundation of China (Grant No. 91852103) and Chinese Government Scholarship. The authors also would like to thank Laboratorio de Informática-Mecánica of Escuela Politécnica Nacional.

References

[1] Lintermann A 2021 Computational Meshing for CFD Simulations *Clinical and Biomedical Engineering in the Human Nose - A Computational Fluid Dynamics Approach* (Springer, Singapore) pp 85–115
[2] Fabritius B and Tabor G 2016 Improving the quality of finite volume meshes through genetic optimisation *Eng. with Comput.* **32** 425–40
[3] Sbardella L, Sayma A I and Imregun M 2000 Semi-structured meshes for axial turbomachinery blades *Int. J. Numer. Meth. Fluids* **32** 569–84
[4] Tomita J T, da Silva L M and da Silva D T 2012 Comparison between unstructured and structured meshes with different turbulence models for a high pressure turbine application *Proc. ASME Turbo Expo* **8** 1633–45
[5] Sitaraman J, Katz A, Jayaraman B, Wissink A M and Sankaran V 2008 Evaluation of a multi-solver paradigm for CFD using overset unstructured and structured adaptive cartesian grids *46th AIAA Aerosp. Sci. Meet. Exhib.*
[6] Mathur S R and Murthy J Y 1997 A pressure-based method for unstructured meshes *Numer. Heat Transf. Part B Fundam. An Int. J. Comput. Methodol.* **31** 195–215

[7] Menter F R and Egorov Y 2010 The scale-adaptive simulation method for unsteady turbulent flow predictions. Part 1: Theory and model description *Flow, Turbul. Combust.* **85** 113–38
[8] Xu C Y, Zhang T, Yu Y Y and Sun J H 2019 Effect of von Karman length scale in scale adaptive simulation approach on the prediction of supersonic turbulent flow *Aerosp. Sci. Technol.* **86** 630–9
[9] Hidalgo V, Escaler X, Valencia E, Peng X, Erazo J, Puga D and Luo X 2019 Scale-adaptive simulation of unsteady cavitation around a Naca66 hydrofoil *Appl. Sci.* **9** 3696
[10] Ji B, Luo X and Wu Y 2014 Unsteady cavitation characteristics and alleviation of pressure fluctuations around marine propellers with different skew angles *J. Mech. Sci. Technol.* **28** 1339–48
[11] Morgut M, Nobile E and Biluš I 2011 Comparison of mass transfer models for the numerical prediction of sheet cavitation around a hydrofoil *Int. J. Multiph. Flow* **37** 620–6
[12] Puga D, Hidalgo V and Luo X 2022 2D structured mesh for simulations of unsteady cavitation around a plane convex hydrofoil *16th Asian Int. Conf. Fluid Machinery J. Phys.: Conf. Ser.* **2217** 012024
[13] Hidalgo V, Suárez G, Erazo J, Puga D, Márquez D, Benavides I, Cando E, Valencia E and Luo X 2021 Numerical study of flow behavior in a cavitation tunnel using RANS with scale-adaptive simulation (SAS) turbulence model in an OpenFOAM framework *30th IAHR Symp. on Hydraulic Machinery and Systems IOP Conf. Ser.: Earth Environ. Sci.* **774** 012023
[14] Hidalgo V, Luo X and Yu A 2014 Cavitating flow simulation with mesh development using Salome open source software *Proc. 11th Int. Conf. Hydrodynamics*
[15] Ariff M, Salim S M and Cheah S C 2009 Wall y+ approach for dealing with turbulent flow over a surface mounted cube Part 1 - low Reynolds number *7th Int. Conf. on CFD in the Minerals and Process Industries*
[16] Popovac M and Hanjalic K 2007 Compound wall treatment for RANS computation of complex turbulent flows and heat transfer *Flow Turbulence Combust* **78** 177
[17] Stimpson C J, Ernst C D, Knupp P, Pébay P P and Thompson D 2007 *The Verdict Geometric Quality Library*
[18] Le Q, Franc J P and Michel J M 1993 Partial cavities: Global behavior and mean pressure distribution *ASME J. Fluids Eng.* **115** 243-8
[19] Escaler X, Farhat M, Avellan F and Egusquiza E 2003 Cavitation erosion tests on a 2D hydrofoil using surface-mounted obstacles *Wear* **254** 441–9